Powder Technology 245 (2013) 227–232

Contents lists available at SciVerse ScienceDirect

Powder Technology

journal homepage: www.elsevier.com/locate/powtec

Yellow–colored mesoporous pure titania and its high stability in visible light photocatalysis

Yanlong Tian, Binbin Chang, Jie Fu, Fengna Xi, Xiaoping Dong *

Department of Chemistry, School of Sciences, Zhejiang Sci-Tech University, 928 Second Avenue, Xiasha Higher Education Zone, Hangzhou, China

ARTICLE INFO

Article history:
Received 12 October 2012
Received in revised form 2 April 2013
Accepted 19 April 2013
Available online 30 April 2013

Keywords:
Mesoporous structure
Nanocrystals
Nanosheets
Composite

ABSTRACT

Yellow–colored pure titania with a mesoporous structure was prepared by the aggregate of titania nanocrystals, which were stabilized by exfoliated titanate nanosheets via an electrostatic interaction. X–ray diffraction patterns and images of transmission electron microscope confirm that titanate sheets are randomly dispersed into the assembled titania nanocrystals without forming any self–restacked phase. This nanocrystals–nanosheets composite exhibits a mesoporous structure with pore size of ~6.5 nm and surface area of 236.3 $m^2\ g^{-1}$. Greatly different from the UV–responded properties of titania nanocrystals and titanate nanosheets, the absorption edge of nanocomposite red–shifts to visible light region. The visible light photocatalytic tests demonstrate that this nanocomposited titania shows excellent activity for the degradation of organic dyes, as well as a colorless organic pollutant of 2, 4–dichlorophenol. The possible photocatalytic mechanism that photogenerated holes as the mainly oxidant species in photocatalysis is proposed based on the trapping experiments of hydroxyl radicals or photogenerated holes. Moreover, as the nanocomposite depicts an extreme stability, no obvious deactivation occurs after five cycles.

1. Introduction

In recent years, semiconductor photocatalysis has received considerable attention since it holds promising potential in both energy and environmental fields [1–3]. Among various semiconductors, titania is most widely used because of its nontoxicity, chemical stability, water insolubility, low price, and favorable photochemical property [4,5]. However, titania can only be excited by ultraviolet (UV) light due to its large band gap of 3.2 eV. Given that UV light only accounts for a small fraction (<5%) of the solar spectrum, thus, its overall efficiency remains too low under natural light irradiation. Moreover, its quantum efficiency is further limited owning to the high recombination rate of photogenerated electron–hole pairs [6,7]. Therefore, designing, fabricating, and tailoring the optical and physicochemical properties of titania are necessary to enhance its absorption in visible region thus to realize the purpose of solar energy derived applications of titania.

Over the last few decades, enormous efforts have been devoted to realize visible light harvesting capability of titania [8–11,14–19]. Doping with metal or nonmetal elements is the most used method that has successfully extended its absorption to visible light range [8–11]. However, impurity elements may act as charge carrier recombination centers, which would reduce the photocatalytic efficiency of material [12]. For example, Wang et al. have confirmed that titania doped with nitrogen can efficiently improve its activity under visible light irradiation, but remarkably lowers its UV light activity [13]. Dye–sensitization is another effective approach to enhance the visible light absorption of titania [14–16]. Unfortunately, it is a fact that appropriate sensitizing dyes are extremely rare, and meanwhile as organic species, they are unstable with respect to chemical and photochemical attacks, which would affect the photocatalytic performance of photocatalyst. Coupling with narrow band gap semiconductors has been reported to effectively improve the visible light catalytic activity of titania [17–19]. Such a combination not only enhances the visible light absorption, but also promotes the separation of photogenerated electron–hole pairs. However, these narrow band gap semiconductors, such as sulfides, are very unstable toward photocorrosion that is not propitious for their long–term use. In addition, both dyes and narrow band gap semiconductors would detach from the surface of titania, which reduces the activity of photocatalyst and meanwhile brings a secondary pollution to the environment. Therefore, great efforts remain to be drawn on the exploitation of "pure" titania materials that respond to visible light [12,20–22]. Most recently, Ye's group developed a novel titania photocatalyst by the bonding assembly of titania nanocrystals (TNCs), which exhibits a narrowed band gap and greatly enhanced visible and solar photocatalysis in comparison with individual TNCs [23]. Nevertheless, the main drawback of this doping–free material is that its visible light response disappears rapidly when it is dispersed into aqueous solution or crushed into a powder. Moreover, the long–term

* Corresponding author. Tel.: +86 571 86843228; fax: +86 571 86843653.
E-mail address: xpdong@zstu.edu.cn (X. Dong).

0032-5910
http://dx.doi.org/10.1016/j.powtec.2013.04.036

exposure in air at room temperature would also make this material slowly fade to whiteness. Therefore, improving the stability of assembled TNCs is very important for its practical application.

Electrostatic aggregate of exfoliated titanate nanosheets (TNSs) bearing negative charges with positively charged nanoparticles has been widely studied, which always forms porous structures [24–30]. The structure of assembled system of TNSs and nanoparticles is strongly dependent on the ratio of nanoparticles to TNSs, from nanoparticles–pillared layered structure to disordered mesoporous structure with the increase of ratio [31,32]. The electrostatic assembly of TNSs and titania nanoparticles has been deeply investigated, including structural properties and UV–responsed photocatalytic performance [33,34]. However, in these reports attentions were focused on the interaction of nanoparticles and TNSs, and the aggregate of incorporated nanoparticles was omitted.

Herein, we reported a yellow–colored pure titania material with a high stability. The titania nanocomposite was prepared via incorporating TNCs into TNSs by the electrostatic interaction, and the followed aggregate of incorporated TNCs by ethanol treating. The resulting TNCs–TNSs nanocomposite possesses a mesoporous structure and enhanced visible light response, which make it show an excellent photocatalytic activity for degrading organic pollutants under visible light irradiation. Moreover, because the assembled TNCs are stabilized by TNSs, the TNCs–TNSs photocatalyst exhibits a high stability and durability during five successive cycles. In addition, the possible photocatalytic mechanism of this material was also discussed.

2. Experimental section

2.1. Synthesis

All reagents were analytical grade and used as received. TNSs were synthesized by delaminating layered protonic titanate (LPT) using ethylamine (EA) aqueous solution as an intercalant, which was described in our previous report [35]. A monodispersed TNCs colloid was prepared by hydrolysis of tetrabutyl titanate using glacial acetic as an inhibitor. In a typical procedure, 10.2 mL of tetrabutyl titanate was slowly added to a mixed solution of glacial acetic acid (12 mL) and distilled water (15 mL) drop by drop under violent stirring. After stirred for 15 min, 30 mL of distilled water was slowly added and then stirred for another 3 h.

The TNCs–TNSs photocatalyst was obtained by the incorporation of TNCs into TNSs. Typically, the TNCs colloid was slowly added to the suspension of TNSs in the molar ratio of $[Ti]_{TNCs}/[Ti]_{TNSs}$ being 3:1. After the mixture was continuously stirred for 12 h, the white precipitate (WP) was collected by centrifugation, washed with absolute ethanol thoroughly, and finally dried at 100 °C overnight. The resulting yellow product was ground for further use.

2.2. Characterization

X–ray diffraction (XRD) patterns were monitored by a DX–2700 diffractometer (Dandong Haoyuan Instrument Co. Ltd., China) using Cu $K\alpha$ radiation ($\lambda = 0.15418$ nm). A scanning electron microscope (SEM, Hitachi S–4800) was used to characterize the morphology of samples. Transmission electron microscope (TEM) images were obtained on a JEOL JEM–2100 electron microscope with an accelerating voltage of 200 kV. Thermogravimetric (TG) data was performed from ambient temperature to 800 °C in flowing N_2 at a rate of 10 °C min^{-1} on a PE Instruments Pyris Diamond 1 thermalanalyzer. Diffuse reflectance spectra were recorded on a Shimadzu 2450 UV–vis spectrometer with an integrating sphere using $BaSO_4$ as the reference. The adsorption/desorption isotherms of nitrogen at 77 K were measured using a Micromeritics ASAP 2020 accelerated surface area and porosimetry analyzer.

2.3. Photocatalytic tests

Visible light photocatalytic activities of photocatalysts were examined by the degradation of methyl orange (MO) in aqueous solution. In each test, 50 mg of catalyst was suspended in an aqueous solution (5 mg L^{-1}, 100 mL) of MO in a quartz glass reactor, which was cooled by recycled water to prevent the thermal catalytic effect. Prior to illumination, the suspension was stirred in the dark for 1 h to ensure the establishment of adsorption–desorption equilibrium of MO on the surface of photocatalyst. A 300 W xenon lamp (HSX–F300, Beijing NBet) equipped with a combination of two glass filters to obtain a wavelength range of 420–780 nm was used as the light source. At given irradiation time intervals, 4 mL of the suspension was extracted and subsequently centrifuged to remove the catalyst particles. The concentration of MO solution was analyzed by measuring the maximum absorbance at 464 nm using a Shimadzu UV-2450 spectrophotometer.

3. Results and discussions

3.1. Characterization of NCs–TNSs

Fig. 1 shows the powder XRD patterns of LPT, EA–intercalated titanate, TNCs, and TNCs–TNSs. The pristine LPT is well crystalline and all of these diffraction peaks can be indexed as the lepidocrocite–like layered structure, in accordance with the literature [36]. Before the reaction with TNCs colloid, the LPT was first intercalated with EA and subsequent exfoliated into TNSs via an osmotic swelling process [37]. Drying the TNSs suspension without adding TNCs colloid results in the formation of EA–intercalated form. The well–developed (0k0) peaks indicate that EA is intercalated between the TNSs to form a turbostatic lamellar structure with the interlayer space of 1.03 nm. Upon reacting TNSs with TNCs colloid, these peaks corresponding to the protonic phase and EA–intercalated phase disappear and give place to three broad peaks at 25.6°, 37.9° and 48.1°, which can be indexed as the anatase (JCPDS 21-1272). This indicates that TNSs are randomly dispersed into assembled TNCs without forming any layered phases. The average particle size of TNCs in the nanocomposite estimated by the Scherrer equation is ~4.6 nm, in accordance with that of the precursor TNCs, as shown in Fig. 1d, which suggests that the aggregate process would not influence the crystal size and phase of the stabilized TNCs.

The morphology and microstructure of the samples were investigated by SEM and TEM. The LPT (Fig. 2a) exhibits a plate–like morphology with well–ordered layered structure. After exfoliation and subsequent restacking with TNCs colloid, a disorganized microtexture can be observed (Fig. 2b). This should be attributed to the random hybridization of TNSs with TNCs, which also brings a porous structure. This structure is favorable for the adsorption and transfer of guest

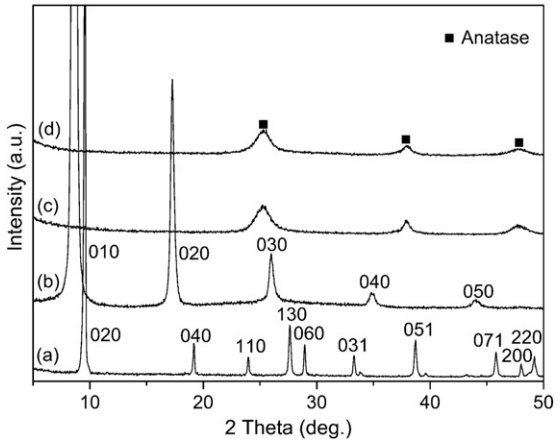

Fig. 1. XRD patterns of (a) LPT, (b) self-restacked form (EA-intercalated titanate), (c) TNCs–TNSs, and (d) TNCs.

species in the catalyst system, resulting in an improved photocatalytic activity. The TEM image of TNCs–TNSs sample (Fig. 2c) displays two distinct images, lines and spherical shapes. The former represents TNSs and the latter is TNCs respectively, which further confirms the random hybridization of TNSs with TNCs. The thickness of single TNS is ~0.8 nm, in accordance with the reported values [38]. The observed size of TNCs is ~5 nm, in good agreement with that determined by XRD analysis. Fig. 2d shows the HR-TEM image of TNCs–TNSs that exhibits a lattice fringe of ~0.35 nm, belonging to the (101) crystallographic plane of anatase titania. The exposed (101) facets would bring a high photocatalytic activity for the degradation of organic pollutants [39]. In addition, the closely connected TNCs also demonstrates the aggregate of TNCs with the immobilization of TNSs.

The nitrogen adsorption–desorption isotherm of TNCs–TNSs sample is shown in Fig. 3. The adsorption isotherm can be classified into the type IV isotherm, which is characteristic for mesoporosity materials. According to the fitting analysis of the BET equation, the surface area of TNCs–TNSs sample is 236.3 $m^2\ g^{-1}$. The hysteresis loop resembles of the TNCs–TNSs sample can be assigned as H3 in the IUPAC classification, indicating the presence of open slit-shaped pores with very wide bodies and narrow short necks [40]. This mesoporous structure should originate from the random hybridization of TNSs with TNCs, as described above. The inset of Fig. 3 displays the pore size distribution of TNCs–TNSs. The obtained diameter of ~6.5 nm is large enough for the access of organic molecules, which is beneficial for the improvement of photocatalytic activity.

The composition of TNCs–TNSs sample was further characterized by TG analyses (Fig. S1). The TG curves of both WP and TNCs–TNSs can be divided into three temperature steps. The first step up to about 150 °C is certainly due to the dehydration of adsorbed water molecules on the surface of nanocomposites [34]. The second domain between 150 °C and 425 °C can be attributed to the loss of structural water molecules associated with TNCs [29]. The loss weights are 7.27% and 5.83% for WP and TNCs–TNSs, respectively. This difference obviously demonstrates that the assembly process of TNCs can remove some of the water molecules' water between TNCs. Finally, the third step above 425 °C is owing to the decomposition of the residual organic group in the interlayer space of nanocomposites [30].

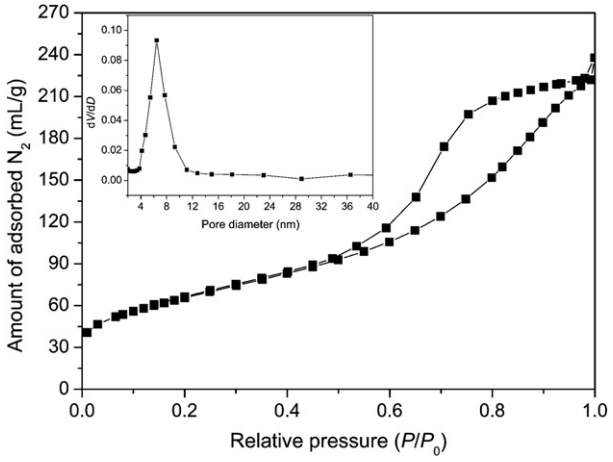

Fig. 3. Nitrogen adsorption–desorption isotherms for the TNCs–TNSs. The inset shows the pore size distribution curve.

Fig. 4 shows the UV–vis diffuse reflectance spectra of TNCs–TNSs, together with the TNSs and TNCs. The TNSs holds an absorption edge of ~308 nm, corresponding to a band gap of ~4.03 eV, and the onset wavelength of ~396 nm of TNCs is related to a band gap of ~3.13 eV. Thus, both the two titania materials are inactive in visible light. However, for the TNCs–TNSs sample, an add–on shoulder is observed in the wavelength of 400–500 nm which is consistent with the yellow color characteristic, as the inset of Fig. 4 shows. According to the

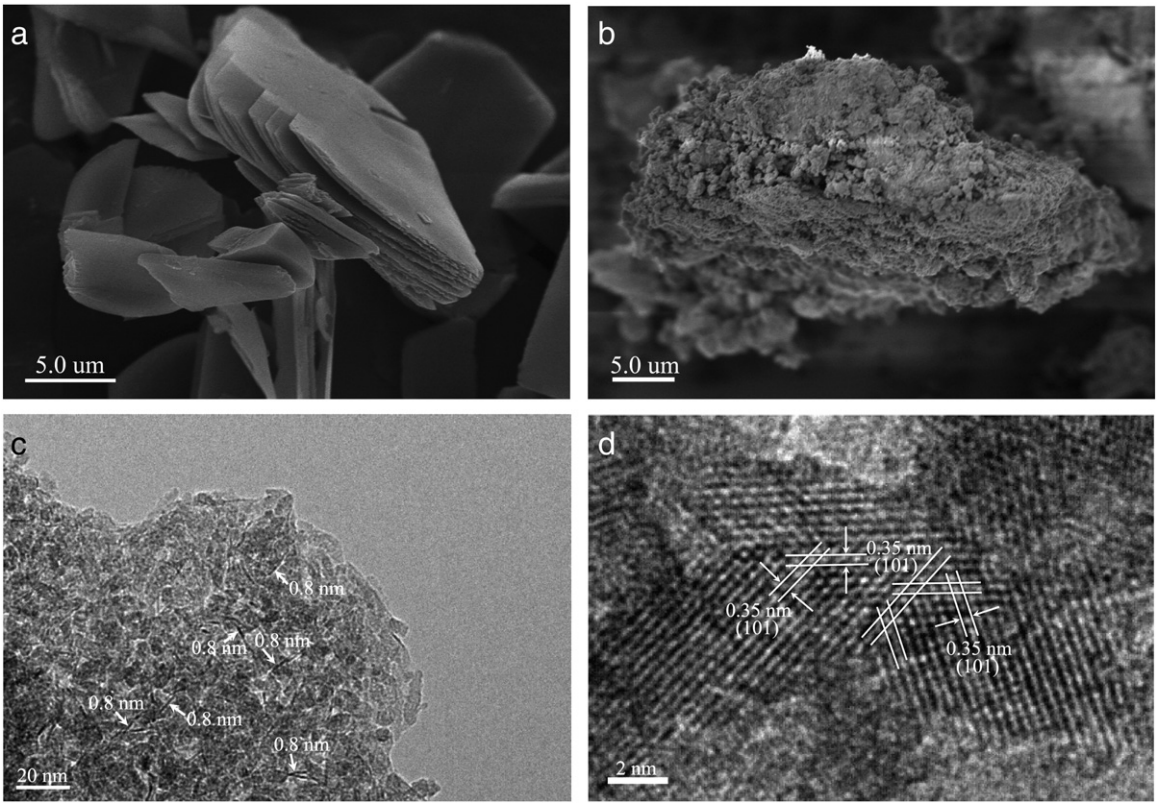

Fig. 2. SEM images of (a) LPT, and (b) TNCs–TNSs; TEM image (c) and HR-TEM image (d) of TNCs–TNSs.

literature, the intercalation of TNCs into the interlayer of layered titanate did not extend the optical absorption to visible region [34]. Similar behavior was also observed in our case, the WP immediately forming by adding TNCs colloid to TNSs suspension. These indicate that the interaction between TNCs and TNSs is not responsible for the enhanced visible absorption of the resultant nanocomposite. However, after ethanol washing and drying the color of TNCs–TNSs nanocomposite gradually changed to yellow, which should be related to the aggregate process of TNCs as water between TNCs was removed. It is noteworthy that the visible optical property of our TNCs–TNSs nanocomposite is really stable, compared with the simply assembled TNCs reported by Ye's group [23]. TNCs–TNSs in our study can still remain its color even under the finely grinding, dispersion in water or long-term exposure in air. This should be attributed to the immobilization of TNCs by TNSs that prevents the dispersion of TNCs during the grinding process or the intercalation of water.

3.2. Photocatalytic study of the NCs–TNSs

To evaluate the photocatalytic activity of as–synthesized nanocomposite photocatalyst, we have investigated the photodegradation of MO under visible light irradiation. As shown in Fig. 5a, the characteristic absorption peak of MO at 463 nm significantly deceases with the increase of irradiation time, and nearly disappears after 3 h. In the meantime, no additional absorption appearing implies the complete decomposition of MO. No change in the absorbance of MO solution is observed in the absence of catalysts (Fig. 5b) suggesting that the MO molecules are quite stable, which excludes the possibility of photolysis in the present system. Actually, the sensitization of dyes cannot be neglected to estimate the photocatalytic activity of semiconductor for the decomposition of dye under visible light. To investigate the effect of dye–sensitization, the photocatalytic performances of LPT, TNCs and a commercial TiO_2 of P25 were also carried out. No apparent degradation on LPT and a slight enhancement of degradation ratio on TNCs and P25 are observed, which suggests that in this condition the dye-sensitization is inconspicuous. In contrast, 95% of MO molecules are decomposed under the same condition as TNCs–TNSs is used, and its rate constant of ~1.509×10^{-2} min^{-1} is nearly 6.3 and 5.6 times larger than those of P25 and TNCs, respectively (Fig. S2). Therefore, the excellent performance of TNCs–TNSs for decomposing MO under visible light irradiation should be ascribed to its significant photocatalytic activity. To further demonstrate the photocatalytic activity of TNCs–TNSs under visible light irradiation, we tested the degradation of 2, 4-dichlorophenol (2, 4–DCP) that has no absorption in the visible light region. As shown in Fig. S3, 2, 4-DCP was effectively degraded over the NCs–TNSs catalyst under visible light irradiation, indicating the highly photocatalytic activity of TNCs–TNSs in visible light.

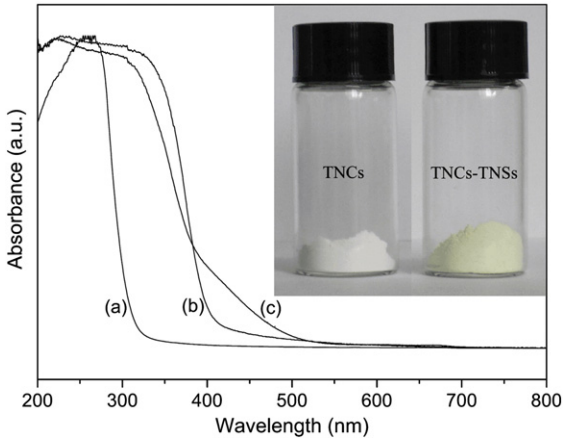

Fig. 4. UV–vis diffuse reflectance spectra of (a) TNSs, (b) TNCs, and (c) TNCs–TNSs. The inset shows a photograph comparing TNCs and TNCs–TNSs.

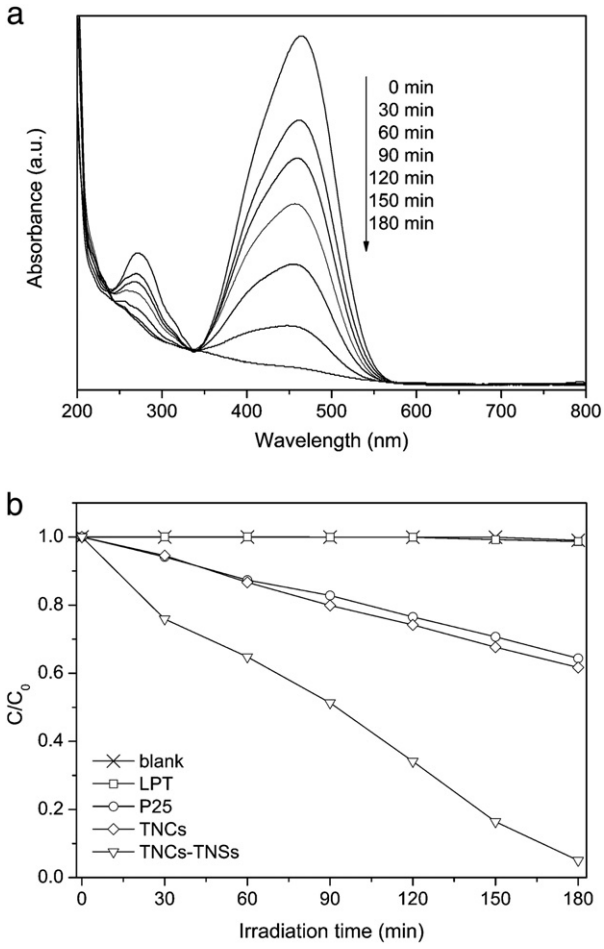

Fig. 5. (a) Absorption spectra of MO with irradiation time over TNCs–TNSs catalyst; (b) Degradation rates of MO under visible light irradiation without catalyst and in the presence of LPT, P25, TNCs, and TNCs–TNSs catalysts.

It is well known that photogenerated holes or hydroxyl radicals are two main species for the oxidization of organic pollutants in aqueous [41]. For investigating the possible photocatalytic mechanism of TNCs–TNSs photocatalyst, we used the trapping experiments of hydroxyl radicals or photogenerated holes to determine the main oxidant species. Disodium ethylenediaminetetraacetate (EDTA) and tertbutyl alcohol (TBA) were respectively used as a hole scavenger and a radical scavenger [42,43]. It is clearly shown that adding TBA did not bring any obvious difference for the degradation behavior of MO, whereas, it was completely suppressed as EDTA was added (Fig. 6). Thus, a possible mechanism with photogenerated holes as the main oxidants was proposed. This result further suggests that dye-sensitization is not the dominant factor for photocatalytic degradation in which hydroxyl radical is the main active species [44–46].

The stability and recyclability of photocatalysts are extremely important for practical applications. No obvious difference of optical and structure properties (not shown) between the fresh and used sample demonstrates that TNCs–TNSs has the high stability during the photocatalytic reaction. Fig. 7 illustrates the relationship between degradation ratio of MO and cycle times, which exhibits a similar degradation behavior in each cycle. Even though the photocatalyst had been recycled for five consecutive cycles, over 80% MO was decomposed with 3 h visible light irradiation. Thus, the stability of assembled TNCs is remarkably enhanced by immobilizing using TNSs.

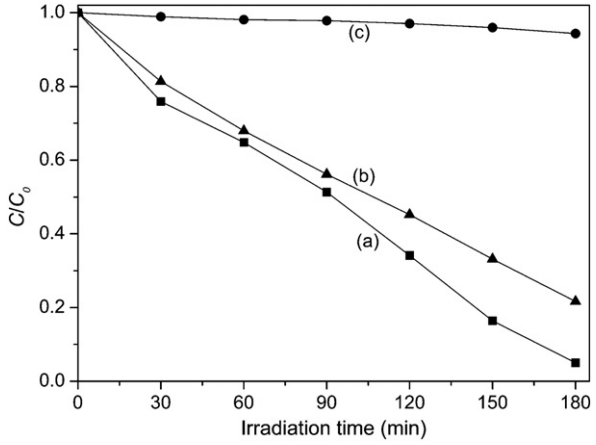

Fig. 6. Photocatalytic degradation of MO over TNCs–TNSs photocatalyst (a) alone, and with the addition of (b) TBA, or (c) EDTA.

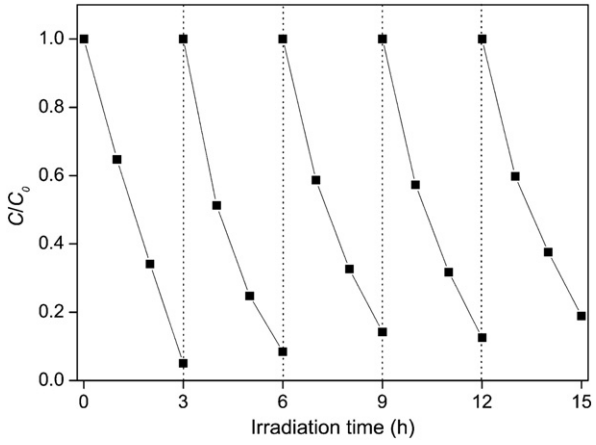

Fig. 7. Cycling runs for the photocatalytic degradation of MO over TNCs–TNSs catalyst under visible light irradiation.

4. Conclusions

In summary, we have successfully developed a yellow–colored pure titania by incorporating TNCs into TNSs, and the followed aggregate of incorporated TNCs using ethanol treating. The electrostatic interaction of TNCs and TNSs results in a mesoporous structure with pore size of ~6.5 nm and surface area of 236.3 $m^2\ g^{-1}$, and the aggregate of TNCs brings the enhanced visible light harvesting capability. There features make the TNCs–TNSs nanocomposite exhibits a highly photocatalytic activity for degradation of organic pollutants. Meanwhile, the immobilization of TNCs using TNSs makes this nanocomposite show the excellent stability and reusability.

Acknowledgments

We greatly acknowledge financial support from the National Natural Science Foundation of China (21001093), the Zhejiang Provincial Natural Science Foundation of China (Y4090285, Y4110418), the Science Foundation of Zhejiang Sci-Tech University (0913840-Y), the Qianjiang Talent Project of Zhejiang Province of China (2011R10048) and the Scientific Research Foundation for the Returned Overseas Chinese Scholars, State Education Ministry.

Appendix A. Supplementary data

Supplementary data to this article can be found online at http://dx.doi.org/10.1016/j.powtec.2013.04.036.

References

[1] A. Fujishima, K. Honda, Electrochemical photolysis of water at a semiconductor electrode, Nature 238 (1972) 37–38.
[2] Z.G. Zou, J.H. Ye, K. Sayama, H. Arakawa, Direct splitting of water under visible light irradiation with an oxide semiconductor photocatalyst, Nature 414 (2001) 625–627.
[3] C.C. Chen, W.H. Ma, J.C. Zhao, Semiconductor-mediated photodegradation of pollutants under visible-light irradiation, Chemical Society Reviews 39 (2010) 4206–4219.
[4] M.R. Hoffmann, S.T. Martin, W. Choi, D.W. Bahnemann, Environmental applications of semiconductor photocatalysis, Chemical Reviews 95 (1995) 69–96.
[5] H.A. Le, L.T. Linh, S. Chin, J. Jurng, Photocatalytic degradation of methylene blue by a combination of TiO_2-anatase and coconut shell activated carbon, Powder Technology 225 (2012) 167–175.
[6] D.E. Skinner, D.P. Colombo, J.J. Cavaleri, R.M. Bowman, Femtosecond investigation of electron trapping in semiconductor nanoclusters, Journal of Physical Chemistry 99 (1995) 7853–7856.
[7] A. Mukherji, B. Seger, G.Q. Lu, L.Z. Wang, Nitrogen doped $Sr_2Ta_2O_7$ coupled with graphene sheets as photocatalysts for increased photocatalytic hydrogen production, ACS Nano 5 (2011) 3483–3492.
[8] R. Asahi, T. Morikawa, T. Ohwaki, K. Aoki, Y. Taga, Visible-light photocatalysis in nitrogen-doped titanium oxides, Science 293 (2001) 269–271.
[9] W. Zhao, C.C. Chen, X.Z. Li, J.C. Zhao, H. Hidaka, N. Serpone, Photodegradation of sulforhodamine-B dye in platinized titania dispersions under visible light irradiation: influence of platinum as a functional co-catalyst, The Journal of Physical Chemistry B 106 (2002) 5022–5028.
[10] H. Irie, Y. Watanabe, K. Hashimoto, Nitrogen-concentration dependence on photocatalytic activity of $TiO_{2-x}N_x$ powders, The Journal of Physical Chemistry. B 107 (2003) 5483–5486.
[11] X.X. Lin, F. Rong, D.G. Fu, C.W. Yuan, Enhanced photocatalytic activity of fluorine doped TiO_2 by loaded with Ag for degradation of organic pollutants, Powder Technology 219 (2012) 173–178.
[12] A. Naldoni, M. Allieta, S. Santangelo, M. Marelli, F. Fabbri, S. Cappelli, C.L. Bianchi, R. Psaro, V.D. Santo, Effect of nature and location of defects on bandgap narrowing in black TiO_2 nanoparticles, Journal of the American Chemical Society 134 (2012) 7600–7603.
[13] J. Wang, D.N. Tafen, J.P. Lewis, Z.L. Hong, A. Manivannan, M.J. Zhi, M. Li, N.Q. Wu, Origin of photocatalytic activity of nitrogen-doped TiO_2 nanobelts, Journal of the American Chemical Society 131 (2009) 12290–12297.
[14] J. He, G. Benko, F. Korodi, T. Polivka, R. Lomoth, B. Akermark, L. Sun, A. Hagfeldt, V. Sundstrom, Modified phthalocyanines for efficient near-IR sensitization of nanostructured TiO_2 electrode, Journal of the American Chemical Society 124 (2002) 4922–4932.
[15] L. Lucarelli, V. Nadtochenko, J. Kiwi, Environmental photochemistry: quantitative adsorption and FTIR studies during the TiO_2-photocatalyzed degradation of orange II, Langmuir 16 (2000) 1102–1108.
[16] T. Wu, G. Liu, J.C. Zhao, H. Hidaka, N. Serpone, Evidence for H_2O_2 generation during the TiO_2-assisted photodegradation of dyes in aqueous dispersions under visible light illumination, The Journal of Physical Chemistry. B 103 (1999) 4862–4867.
[17] S.F. Chen, L. Chen, S. Gao, G.Y. Cao, The preparation of coupled WO_3/TiO_2 photocatalyst by ball milling, Powder Technology 160 (2005) 198–202.
[18] A. Kumar, A.K. Jain, Photophysics and photochemistry of colloidal CdS–TiO_2 coupled semiconductors-photocatalytic oxidation of indole, Journal of Molecular Catalysis A: Chemical 165 (2001) 265–273.
[19] H.B. Yin, Y. Wada, T. Kitamura, T. Sakata, H. Mori, S. Yanagida, Enhanced photocatalytic dechlorination of 1,2,3,4-tetrachlorobenzene using nanosized CdS/TiO_2 hybrid photocatalyst under visible light irradiation, Chemistry Letters 30 (2001) 334–335.
[20] X.B. Chen, L. Liu, P.Y. Yu, S.S. Mao, Increasing solar absorption for photocatalysis with black hydrogenated titanium dioxide nanocrystals, Science 331 (2011) 746–750.
[21] J. Tao, T. Luttrell, M. Batzill, A two dimensional phase of TiO_2 with a reduced band gap, Nature Chemistry 3 (2011) 296–300.
[22] T.R. Gordon, M. Cargnello, T. Paik, F. Mangolini, R.T. Weber, P. Fornasiero, C.B. Murray, Nonaqueous synthesis of TiO_2 nanocrystals using TiF_4 to engineer morphology, oxygen vacancy concentration, and photocatalytic activity, Journal of the American Chemical Society 134 (2012) 6751–6761.
[23] H. Tong, N. Umezawa, J.H. Ye, Visible light photoactivity from a bonding assembly of titanium oxide nanocrystals, Chemical Communications 47 (2011) 4219–4221.
[24] T.W. Kim, S.G. Hur, S.J. Hwang, H. Park, W. Chio, J.H. Choy, Heterostructured visible-light-active photocatalyst of chromia-nanoparticle-layered titanate, Advanced Functional Materials 7 (2007) 307–314.
[25] T.W. Kim, S.J. Hwang, S.H. Jhung, J.S. Chang, H. Park, W. Choi, J.H. Choy, Bifunctional heterogeneous catalysts for selective epoxidation and visible light driven photolysis: nickel oxide-containing porous nanocomposite, Advanced Materials 20 (2008) 539–542.
[26] Y.L. Tian, J. Fu, B.B. Chang, F.N. Xi, X.P. Dong, Synthesis of mesoporous CdS/titania composites with visible light photocatalytic activities, Materials Letters 81 (2012) 95–98.
[27] T.W. Kim, H.W. Ha, M.J. Paek, S.H. Hyun, J.H. Choy, S.J. Hwang, Unique phase transformation behavior and visible light photocatalytic activity of titanium oxide hybridized with copper oxide, Journal of Materials Chemistry 20 (2010) 3238–3245.
[28] H.W. Ha, T.W. Kim, J.H. Choy, S.J. Hwang, Relationship between electrode performance and chemical bonding nature in mesoporous metal oxide-layered titanate nanohybrids, Journal of Physical Chemistry C 113 (2009) 21941–21948.

[29] F. Kooli, T. Sasaki, V. Rives, M. Watanabe, Synthesis and characterization of a new mesoporous alumina-pillared titanate with a double-layer arrangement structure, Journal of Materials Chemistry 10 (2000) 497–501.
[30] J.W. Kim, H.W. Ha, M.J. Paek, S.H. Hyun, Il-H. Baek, J.H. Choy, S.J. Hwang, Mesoporous iron oxide-layered titanate nanohybrids: soft-chemical synthesis, characterization, and photocatalyst application, Journal of Physical Chemistry C 112 (2008) 14853–14862.
[31] J.H. Choy, H.C. Lee, H. Jung, H. Kim, H. Boo, Exfoliation and restacking route to anatase-layered titanate nanohybrid with enhanced photocatalytic activity, Chemistry of Materials 14 (2002) 2486–2491.
[32] S.M. Paek, H. Jung, Y.J. Lee, M. Park, S.J. Hwang, J.H. Choy, Exfoliation and reassembling route to mesoporous titania nanohybrids, Chemistry of Materials 18 (2006) 1134–1140.
[33] J.H. Choy, H.C. Lee, H. Jung, S.J. Hwang, A novel synthetic route to TiO_2-pillared layered titanate with enhanced photocatalytic activity, Journal of Materials Chemistry 11 (2001) 2232–2234.
[34] Z.J. Chen, B.Z. Lin, B.H. Xu, X.L. Li, Q.Q. Wang, K.Z. Zhang, M.C. Zhu, Preparation and characterization of mesoporous TiO_2-pillared titanate photocatalyst, Journal of Porous Materials 18 (2011) 185–193.
[35] J. Fu, Y.L. Tian, B.B. Chang, G.N. Li, F.N. Xi, X.P. Dong, Synthesis of Mn-intercalated layered titanate by exfoliation–flocculation approach and its efficient photocatalytic activity under visible-light, Journal of Solid State Chemistry 196 (2012) 282–287.
[36] T. Sasaki, F. Kooli, M. Iida, Y. Michiue, S. Takenouchi, Y. Yajima, F. Izumi, B.C. Chakoumakos, M. Watanabe, A mixed alkali metal titanate with the Lepidocrocite-like layered structure. preparation, crystal structure, protonic form, and acid–base intercalation properties, Chemistry of Materials 10 (1998) 4123–4128.
[37] T. Sasaki, M. Watanabe, Osmotic swelling to exfoliation. Exceptionally high degrees of hydration of a layered titanate, Journal of the American Chemical Society 120 (1998) 4682–4689.
[38] T. Sasaki, M. Watanabe, H. Hashizume, H. Yamada, H. Nakazawa, Macromolecule-like aspects for a colloidal suspension of an exfoliated titanate. Pairwise association of nanosheets and dynamic reassembling process initiated from it, Journal of the American Chemical Society 118 (1996) 8329–8335.
[39] Z.G. Xiong, X.S. Zhao, Nitrogen-doped titanate-anatase core–shell nanobelts with exposed 101 anatase facets and enhanced visible light photocatalytic activity, Journal of the American Chemical Society 134 (2012) 5754–5757.
[40] K.S.W. Sing, D.H. Everett, R.A.W. Haul, L. Moscou, R.A. Pierotti, J. Rouquerol, T. Siemieniewska, Reporting physisorption data for gas/solid systems with special reference to the determination of surface area and porosity, Pure and Applied Chemistry 57 (1985) 603–619.
[41] T. Tachikawa, M. Fujitsuka, T. Majima, Mechanistic insight into the TiO_2 photocatalytic reactions: design of new photocatalysts, Journal of Physical Chemistry C 111 (2007) 5259–5275.
[42] M.S. Elovitz, U. Von Gunten, Hydroxyl radical/ozone ratios during ozonation processes. I. The Rct concept, Ozone Science and Engineering 21 (1999) 239–260.
[43] C. Minero, G. Mariella, V. Maurino, D. Vione, E. Pelizzetti, Photocatalytic transformation of organic compounds in the presence of inorganic ions. 2. Competitive reactions of phenol and alcohols on a titanium dioxide–fluoride system, Langmuir 16 (2000) 8964–8972.
[44] G.M. Liu, X.Z. Li, J.C. Zhao, S. Horikoshi, H. Hidaka, Photooxidation mechanism of dye alizarin red in TiO_2 dispersions under visible illumination: an experimental and theoretical examination, Journal of Molecular Catalysis A: Chemical 153 (2000) 221–229.
[45] D. Jiang, Y. Xu, D. Wu, Y.H. Sun, Visible-light responsive dye-modified TiO_2 photocatalyst, Journal of Solid State Chemistry 181 (2008) 593–602.
[46] L. Pan, J.J. Zou, X.W. Zhang, L. Wang, Water-mediated promotion of dye sensitization of TiO_2 under visible light, Journal of the American Chemical Society 133 (2011) 10000–10002.